International Conference on Mathematics and Computational Methods Applied to Nuclear Science and Engineering (M&C 2011)
Rio de Janeiro, RJ, Brazil, May 8-12, 2011, on CD-ROM, Latin American Section (LAS) / American Nuclear Society (ANS)
ISBN 978-85-63688-00-2

THE SPECTRAL VOLUME METHOD AS APPLIED TO TRANSPORT PROBLEMS

Ryan G. McClarren
Dept. of Nuclear Engineering
Texas A&M University
3133 TAMU
College Station, TX 77843-3133
rgm@tamu.edu

ABSTRACT

We present a new spatial discretization for transport problems: the spectral volume method. This method, first developed by Wang for computational fluid dynamics, divides each computational cell into several sub-cells and enforces particle balance on each of these sub-cells. Also, these sub-cells are used to build a polynomial reconstruction in the cell. The idea of dividing cells into many cells is a generalization of the simple corner balance and other similar schemes. The spectral volume method preserves particle conservation and preserves the asymptotic diffusion limit. We present results from the method on two transport problems in slab geometry using discrete ordinates and second through sixth order spectral volume schemes. The numerical results demonstrate the accuracy and preservation of the diffusion limit of the spectral volume method. Future work will explore possible benefits of the scheme for high-performance computing and for resolving diffusive boundary layers.

Key Words: Deterministic transport, discrete ordinates methods, high-resolution schemes, diffusive boundary layers

1. INTRODUCTION

Discretization techniques for linear particle transport problems often require several spatial degrees-of-freedom per spatial cell. Most often these degrees of freedom are necessary for the method to be robust in the asymptotic diffusion limit [1], or to achieve high-orders of accuracy [2]. Commonly, the need for extra unknowns inside a cell is considered an inconvenience as transport solutions already have more unknowns than other physics in multiphysics problems due to the fact that the phase space for transport is, in general, seven-dimensional. There are, however, advantages to having multiple unknowns per spatial cell. One example is the fact that transport solutions are often smooth in regions of constant cross-sections. If this solution can be captured by high-order reconstructions using large cell sizes, methods that use extra unknowns can be more efficient than low order methods. Also, recent and forthcoming high-performance computing architectures put a premium on minimizing the movement of data. Therefore, if increasing the number of local unknowns does not increase the communication burden, the extra accuracy might come at a marginal extra cost.

Recently, the spectral volume method was introduced for advection and fluid dynamics problems [3–6]. This method divides the solution domain into computational cells in the standard fashion,

and then each of these cells is divided into sub-cells. On each of the sub-cells a local balance equation is solved where the local solution is represented as a polynomial of the same order as the number of sub-cells. Additionally, the number of sub-cells does not affect the amount of communication between cells. The spectral volume method can also be thought of as a generalization of the simple corner balance method and other sub-cell balance methods previously presented in the transport literature [7]. The term spectral is used to refer to the fact that a polynomial reconstruction is used to determine the solution in each cell in a similar manner to a spectral method for a problem with a finite domain. Note that the standard P_N equations for transport are a spectral method in angle.

Another potential application of the spectral volume method is as a subgrid model for resolving boundary layers at the edge of a diffusive region. Most discretizations require resolving a mean-free path to properly resolve boundary layers. Because the spectral volume method solves a balance equation on each sub-cell, if the sub-cells are logarithmically spaced inside a cell so that a mean-free path is resolved at the diffusive boundary, the boundary layer can be properly resolved.

In this work we present the spectral volume method and how to apply it to transport problems. The focus here is on the basics of the method and to demonstrate how it performs. To this end we treat steady problems using discrete ordinates in te one-speed case with isotropic scattering in slab geometry. We also discuss the important properties of the method, and the necessary future work.

2. THE SPECTRAL VOLUME METHOD IN SLAB GEOMETRY

We begin the derivation of the spectral volume method with the linear, steady-state transport equation in slab geometry under the discrete ordinates approximation [8]:

$$\mu_l \frac{\partial \psi_l}{\partial x} + \sigma_\mathrm{t} \psi_l = \frac{\sigma_\mathrm{s}}{2} \langle \psi_l \rangle + \frac{Q}{2}, \qquad l \in [1, L]. \tag{1}$$

In this equation $x \in [0, X]$ is the spatial variable and $\psi_l(x)$ is the angular flux of particles along a the direction μ_l. The material medium is characterized by a total cross-section $\sigma_\mathrm{t}(x)$ and scattering cross-section $\sigma_\mathrm{s}(x)$, both with units of inverse length; the prescribed source is denoted by $Q(x)$. The quadrature set is comprised of L pairs of directions and weights (μ_l, w_l), and the integration over all angle is denoted using angle brackets

$$\langle \psi_l \rangle = \sum_{l=1}^{L} w_l \, \psi_l \equiv \phi, \tag{2}$$

and the quadrature set is normalized so that $\sum_{l=1}^{L} w_l = 2$. The boundary conditions for Eq. (1) are

$$\psi_l(0) = f_l \text{ for } \mu_l > 0, \quad \psi(X) = g_l \text{ for } \mu_l < 0, \tag{3}$$

Now we partition the spatial domain into N non-overlapping cells. The i^{th} such cell has a width $\Delta x_i = x_{i+1/2} - x_{i-1/2}$, and the point $x_{i+1/2}$ is the interface between cell i and cell $i+1$. We then further partition each cell i into K sub-cells of width $\Delta x_{i,k}$, and denote this sub-cell using

i,k and its left and right edges as $x_{i,k-1/2}$ and $x_{i,k+1/2}$ respectively. Averaging Eq. (1) over a generic sub-cell k of cell i yields

$$\frac{\mu_l}{\Delta x_{i,k}}\left(\hat{\psi}_l^{i,k+1/2}-\hat{\psi}_l^{i,k-1/2}\right)+\sigma_{\mathrm{t}}\psi_l^{i,k}=\frac{\sigma_{\mathrm{s}}}{2}\langle\psi_l^{i,k}\rangle+\frac{Q^{i,k}}{2}, \tag{4}$$

where we have denoted ψ_l averaged over a sub-cell as

$$\psi_l^{i,k}=\int_{x_{i,k-1/2}}^{x_{i,k+1/2}}\psi_l\,dx. \tag{5}$$

The material properties and source in general differ from cell to cell, but in the interest of notational simplicity we have not explicitly shown this in Eq. (4).

We have yet to detail the interfacial values of the angular flux, $\hat{\psi}_l^{i,k\pm1/2}=\psi_l(x_{i,k\pm1/2})$. To determine these interfacial values we treat the sub-cell averages as the value in the middle of the sub-cell, $\psi_l^{i,k}\approx\psi_l(x_{i,k})$ and then fit a Lagrange polynomial through these points. This polynomial is given by

$$p_l(x)=\sum_{k=1}^{K}\varphi_k(x)\psi_l^{i,k}, \tag{6}$$

where

$$\varphi_k(x)=\prod_{q=1,q\neq k}^{K}\frac{x-x_{iq}}{x_{i,k}-x_{iq}}. \tag{7}$$

We then use this polynomial to give the value of the ψ_l inside of cell i. Specifically, this polynomial gives the interfacial values between the sub-cells:

$$\hat{\psi}_l^{i,k+1/2}=p_l(x_{i,k+1/2})\qquad\text{for } k\in[2,K-1]. \tag{8}$$

At the interface between cells we use the principle of upwinding to choose the value[1]. Specifically,

$$\hat{\psi}_l^{i,k-1/2}=\begin{cases}p_l(x_{i-1/2}) & \mu_l<0\\ p_l^{i-1}(x_{i-1/2}) & \mu_l>0\end{cases}\quad\text{for } k=1, \tag{9}$$

and

$$\hat{\psi}_l^{i,k+1/2}=\begin{cases}p_l^{i+1}(x_{i+1/2}) & \mu_l<0\\ p_l(x_{i+1/2}) & \mu_l>0\end{cases}\quad\text{for } k=K, \tag{10}$$

where p_l^i is the interpolation polynomial for cell i.

We have now fully described the discretization in space. We have provided a prescription to divide the spatial domain into cells, then further dividing those cells into sub-cells, and fitting a polynomial using the averages of the sub-cells to describe the variation of the solution inside each cell. This method is the spectral volume method [3–6]. In the original description of this scheme the main cells are referred to as spectral volumes because inside of these cells we spectrally reconstruct the function values.

[1]Upwinding simply means that at cell interfaces we move information in the proper direction. In discrete ordinates this means we enforce that when μ_l is positive, information moves exclusively from left to right at the interface. When μ_l is negative, we move information from right to left. In more other systems where the direction of information flow is more difficult to discern (e.g. in the P_N equations or in fluid dynamics), one solves a Riemann problem to upwind information at cell interfaces.

2.1 CHOICE OF SUB-CELL PARTIONING

We have yet to address the question of how to partition the cell into sub-cells. The most straightforward way to partition the cell is to make each sub-cell the same size: $\Delta x_{i,k} = \Delta x_i/K$. Unfortunately, this approach will lead to a non-convergent method for high-order elements [5]. This phenomenon is due to the fact that the interpolating polynomials are highly oscillatory near the cell-edges, and is an example of the Runge phenomenon.

Using Gauss-Lobatto quadrature points to define the sub-cell edges has been shown to maintain convergence [5]. For a generic cell this approach leads to the sub-cell edges

$$x_{i,k+1/2} = \frac{\Delta x_i}{2}\left(1 - \cos\left(\frac{k\pi}{K}\right)\right), \quad k = 0, \ldots, K. \tag{11}$$

The values of these edges are given in Table I for several values of K. Notice how the sub-cells are clustered near the edges of the cell. This is the reason that Gauss-Lobatto quadrature maintains convergence: by clustering the points near the edges of the cell, oscillations near the cell edges are minimized at the cost of losing accuracy in the middle of the cell.

Table I: Sub-cell edges defined by Gauss-Lobatto points for a cell with $\Delta x_i = 1$

K	Points
2	0, 0.5, 1
3	0, .25, .75, 1
4	0, 0.146447, 0.5, 0.853553, 1
5	0, 0.0954915, 0.345492, 0.654508, 0.904508, 1
6	0, 0.0669873, 0.25, 0.5, 0.75, 0.933013, 1
7	0, 0.0495156, 0.188255, 0.38874, 0.61126, 0.811745, 0.950484, 1

Another possible way to define the sub-cells is to use logarithmic spacing in order to resolve a boundary layer. This is, perhaps, an attractive approach to resolving diffusive boundary layers as one can make the sub-cell widths resolve a mean-free path near a change in cross-section. Such sub-cell partitioning makes sense when different cells have different partitions, and will be the subject of future work.

3. PROPERTIES OF THE SPECTRAL VOLUME METHOD

Conservation

The spectral volume method can easily be shown to be conservative because we have defined the interfacial values to be continuous between sub-cells. If we multiply Eq. (4) by $\Delta x_{i,k}/\Delta x_i$ and sum over $k = 1 \ldots K$, we get

$$\frac{\mu_l}{\Delta x_i}\left(\hat{\psi}_l^{i,K+1/2} - \hat{\psi}_l^{i,1/2}\right) + \sigma_\mathrm{t}\bar{\psi}_l^i = \frac{\sigma_\mathrm{s}}{2}\langle\bar{\psi}_l^i\rangle + \frac{\bar{Q}^i}{2}, \tag{12}$$

where

$$\bar{\psi}_l^i = \sum_{k=1}^{K} \frac{\Delta x_{i,k}}{\Delta x_i} \psi_l^{i,k}, \tag{13}$$

with $\bar{Q}^i$ defined in the same manner. Therefore, the method is conservative on each cell. To show conservation over the entire domain, we multiply Eq. (12) by Δx_i and sum over all cells. This gives, using the definitions in Eqs. (9) and (10),

$$-\mu_l \left(\hat{\psi}_l^{I,K+1/2} - f_l \right) + \sum_i \Delta x_i \left(\frac{\sigma_\mathrm{s}}{2} \langle \bar{\psi}_l^i \rangle - \sigma_\mathrm{t} \bar{\psi}_l^i + \frac{\bar{Q}^i}{2} \right) = 0, \quad \mu > 0, \tag{14a}$$

and

$$-\mu_l \left(g_l - \psi_l^{1,1/2} \right) + \sum_i \Delta x_i \left(\frac{\sigma_\mathrm{s}}{2} \langle \bar{\psi}_l^i \rangle - \sigma_\mathrm{t} \bar{\psi}_l^i + \frac{\bar{Q}^i}{2} \right) = 0, \quad \mu < 0. \tag{14b}$$

These equations show that the method is also globally conservative because information entering/leaving the boundary balance the total sources and material interactions.

Accuracy

It can also be shown that when every cell in the domain is divided into K sub-cells, the method is accurate to $O(\Delta x_i^K)$ [5]. This can be easily seen for the case of $K = 1$ because then the method is equivalent to the step scheme [9]. Also, the case of $K = 2$ is equivalent to a corner balance method [7], which are known to be second-order accurate. We can see this by writing out the equations for $\mu > 0$ for a generic cell with $K = 2$ and $\Delta x_i = 2\Delta x_{i,k}$:

$$\frac{\mu_l}{\Delta x_i} \left((\psi_l^{i,2} + \psi_l^{i,1}) - (3\psi_l^{i-1,2} - \psi_l^{i-1,1}) \right) + \sigma_\mathrm{t} \psi_l^{i,1} = \frac{\sigma_\mathrm{s}}{2} \langle \psi_l^{i,1} \rangle + \frac{Q^{i,k}}{2}, \tag{15a}$$

$$\frac{\mu_l}{\Delta x_i} \left((3\psi_l^{i,2} - \psi_l^{i,1}) - (\psi_l^{i,2} + \psi_l^{i,1}) \right) + \sigma_\mathrm{t} \psi_l^{i,2} = \frac{\sigma_\mathrm{s}}{2} \langle \psi_l^{i,2} \rangle + \frac{Q^{i,k}}{2}. \tag{15b}$$

Equation (15) gives a corner balance scheme where the value at the cell-center and at the cell edges are linear interpolations from the sub-cell values.

Adaptivity

The spectral volume method is well-suited to local p-adaptivity where the number of sub-cells varies throughout the problem to resolve features of the solution. This is so because cells only communicate through outflow conditions on the main cells and the number of sub-cells only indirectly affects the outflow. Also, the sub-cell partitioning can be adaptively selected to resolve mean-free paths where desired, as a form of h-adaptivity. Static adaptivity using the spectral volume method has been shown to be successful in results from multidimensional computational fluid dynamics simulations [6]. Furthermore, the interpolation inside each cell can be used to deal with dendritic meshes that arise in adaptive mesh refinement calculations.

High-performance computing

The communication pattern between cells in the spectral volume method is the same for any number of sub-cells. For discrete ordinates problems, each cell requires the incoming flux at each incoming face and communicates its outgoing flux at the appropriate faces. The amount of data is the same regardless of the size of K. Therefore, one can amortize the communication overhead over a larger number of sub-cells. An oft-repeated maxim regarding leading-edge high perfomance computing hardware is "Flops are (nearly) free," meaning that communication and memory are more important than floating point operations per second (Flops). The spectral volume method is able to increase the number of Flops per communication by increasing K. Of course, in discrete ordinates codes, increasing K means increasing the number of points where the scattering source must be stored (one for each sub-cell), and this could be the main obstacle for using spectral volumes in high-performance computing. Other transport schemes, such as spherical harmonics, could eliminate some of these sub-cell unknowns using Schur complements as has been demonstrated in recent magnetohydrodynamics methods [10], possibly making the larger values of K "free".

Diffusion Limit

We will now examine how the spectral volume method behaves in the diffusion limit. The diffusion limit [9, 11, 12] of the linear transport equation refers to the pheonomenon that when scattering dominates streaming, absorption, and sources, the transport equation asymptotically limits to a diffusion equation. Specifically, to leading order the angular flux becomes isotropic (i.e., $\psi = \frac{1}{2}\phi$) and is governed by a diffusion equation:

$$-\frac{d}{dx}\frac{1}{3\sigma_\mathrm{t}}\frac{d\phi}{dx} + \sigma_\mathrm{a}\phi = Q. \tag{16}$$

We will apply the standard asymptotic analysis [9] to the spectral volume scheme by scaling Eq. (4) using a small, positive parameter ϵ. We expect that in the limit of strong scattering and small absorption and sources, the spectral volume method for the transport equation limits to a valid discretization of the diffusion equation. Our analysis will look at regions away from boundaries: we leave analysis of the boundaries for future work. Specifically, we make the replacements

$$\begin{aligned}\sigma_\mathrm{t} &\to \frac{\sigma_t}{\epsilon},\\ \sigma_\mathrm{a} &\to \epsilon\sigma_\mathrm{a},\\ Q &\to \epsilon Q.\end{aligned}$$

Using these replacements, Eq. (4) becomes after some rearrangement

$$\frac{\epsilon\mu_l}{\Delta x_{i,k}}\left(\hat{\psi}_l^{i,k+1/2} - \hat{\psi}_l^{i,k-1/2}\right) + \sigma_\mathrm{t}\psi_l^{i,k} = \frac{1}{2}\left(\sigma_\mathrm{t} - \epsilon^2\sigma_\mathrm{a}\right)\left\langle\psi_l^{i,k}\right\rangle + \frac{\epsilon^2 Q^{i,k}}{2}. \tag{17}$$

We next expand $\psi_l^{i,k}$ in a power series in ϵ:

$$\psi_l^{i,k} = \sum_{j=0}^{\infty}\epsilon^j\psi_l^{(j),i,k}, \tag{18}$$

and equate like orders of ϵ. The $O(1)$ terms of Eq. (17) give that the leading order angular flux is isotropic as in the continuous equations:

$$\psi_l^{(0),i,k} = \frac{1}{2}\langle \psi_l^{(0),i,k} \rangle \equiv \frac{\phi^{(0),i,k}}{2}. \tag{19}$$

Note, $\hat{\psi}_l^{(0),i,k\pm 1/2}$ is also isotropic because $\hat{\psi}_l^{i,k\pm 1/2}$ is a linear combination of the $\psi^{i,k}$. We next take the $O(\epsilon)$ terms in Eq. (17),

$$\frac{\mu_l}{\Delta x_{i,k}} \left(\hat{\psi}_l^{(0),i,k+1/2} - \hat{\psi}_l^{(0),i,k-1/2} \right) + \sigma_\mathrm{t} \psi_l^{(1),i,k} = \frac{1}{2}\sigma_\mathrm{t} \phi^{(1),i,k}, \tag{20}$$

and perform the quadrature sums (i.e., multiply by w_l and sum over l) to get for the $k = 1$ sub-cell

$$\sum_{l=1}^{L} w_l \mu_l \hat{\psi}_l^{(0),i,3/2} - \sum_{\mu_l > 0}^{L} w_l \mu_l \hat{\psi}^{(0),i-1,K+1/2} - \sum_{\mu_l < 0}^{L} w_l \mu_l \hat{\psi}^{(0),i,1/2}, \tag{21a}$$

which simplifies to

$$\hat{\phi}_l^{(0),i,1/2} = \hat{\phi}^{(0),i-1,K+1/2}, \tag{21b}$$

for symmetric quadrature sets. Similarly for the $k = K$ sub-cell we get

$$\hat{\phi}^{(0),i,K+1/2} = \hat{\phi}^{(0),i+1,1/2}. \tag{21c}$$

The equations for $k \neq 1$ or K, that is all the interior sub-cells, all give $0 = 0$ after performing the sums because the flows across interior sub-cell interfaces is independent of the sign of μ_l. Equations (21a) and (21c) show that there is zero net current at the cell interfaces as a consequence of the fact that the lowest order angular flux is isotropic.

We can also multiply Eq. (20) by $w_l \mu_l$ and sum over l to get a discretized Fick's law on each sub-cell:

$$J^{(1),i,k} = -\frac{1}{6\sigma_\mathrm{t} \Delta x_{i,k}} \left(\hat{\phi}^{(0),i,k+1/2} - \hat{\phi}^{(0),i,k-1/2} \right), \tag{22}$$

where

$$J^{i,k} = \langle \mu_l \psi_l^{i,k} \rangle.$$

Equation (21) is needed to derive Eq. (22) because without the conditions in Eq. (21) the value of $\hat{\phi}^{(0),i,k}$ at $k = 1$ and K would be a combination of the scalar flux in the ith cell and it's neighbor due to upwinding at the cell interfaces.

We proceed further by taking the $O(\epsilon^2)$ terms of Eq. (17),

$$\frac{\mu_l}{\Delta x_{i,k}} \left(\hat{\psi}_l^{(1),i,k+1/2} - \hat{\psi}_l^{(1),i,k-1/2} \right) + \sigma_\mathrm{t} \psi_l^{(2),i,k} = \frac{1}{2}\sigma_\mathrm{t} \phi^{(2),i,k} - \frac{1}{2}\sigma_\mathrm{a} \phi^{(0),i,k} + \frac{Q}{2}, \tag{23}$$

Taking this equation for the $(i, 1)$ sub-cell and adding the Eq. (23) for the $(i-1, K)$ sub-cell and then multiplying by w_l and summing over l gives

$$\frac{1}{\Delta x_{i,k}} \left(\hat{J}^{(1),i,3/2} - \hat{J}^{(1),i-1,K-1/2} \right) + \sigma_{\mathrm{a},i} \phi^{(0),i,1} + \sigma_{\mathrm{a},i} \phi^{(0),i-1,2} = Q^{i,1} + Q^{i-1,K}. \tag{24}$$

For $K = 2$, we can simplify Eq. (24) by writing

$$\hat{J}^{(1),i,3/2} = \frac{J^{(1),i,1} + J^{(1),i,2}}{2}, \quad \hat{J}^{(1),i-1,3/2} = \frac{J^{(1),i-1,1} + J^{(1),i-1,2}}{2}, \tag{25}$$

and

$$J^{(1),i,1} = J^{(1),i,2} = -\frac{1}{3\sigma_{\mathrm{t}}\Delta x_i}\left(\phi^{(0),i,2} - \phi^{(0),i,1}\right). \tag{26}$$

Combining Eqs. (24), (25), and (26) gives

$$\frac{2}{\Delta x_i}\left[-\frac{1}{3\sigma_{\mathrm{t},i}\Delta x_i}\left(\phi^{(0),i,2} - \phi^{(0),i,1}\right) + \frac{1}{3\sigma_{\mathrm{t},i-1}\Delta x_{i-1}}\left(\phi^{(0),i-1,2} - \phi^{(0),i-1,1}\right)\right] + \sigma_{\mathrm{a},i}\phi^{(0),i,1} + \sigma_{\mathrm{a},i}\phi^{(0),i-1,2} = Q^{i,1} + Q^{i-1,2}. \tag{27}$$

This is a consistent discretization of the diffusion equation showing that the $K = 2$ spectral volume method is robust in the diffusion limit. For cases of $K > 2$ we will not write out the asymptotic diffusion equation solved by these methods by writing the forms of the first-order currents in Eq. (24) due to their complexity. We do, however, conjecture that these methods will possess the correct asymptotic diffusion limit because 1) these methods are more accurate than the $K = 2$ method and 2) they also have a correct Fick's law and continuity of scalar flux at the cell interfaces. We plan to produce the diffusion equation for general K in future work. In this work we justify our conjecture through numerical results below.

4. NUMERICAL RESULTS

To examine the behavior of numerical results from the spectral volume method, we solved two different problems. One, Reed's problem [13], has several different kinds of material regions, and the other is a highly diffusive problem adapted from a problem in Ref. [9]. We solve both problems using S_8 with Gaussian quadrature on a uniform mesh. To obtain the solutions we use a sweep-based GMRES scheme [14].

Table II: Material Layout in Reed's Problem

Vacuum Boundary	Scattering Region		Vacuum	Absorber	Strong Source	Reflecting Boundary
	$\Sigma_a = 0.1$ $\Sigma_s = 0.9$			$\Sigma_a = 5$ $\Sigma_s = 0$ $Q = 0$	$\Sigma_a = 50$ $\Sigma_s = 0$ $Q = 50$	
	$Q = 0$ $x < 1$	$Q = 1$ $1 < x < 3$	$3 < x < 5$	$5 < x < 6$	$6 < x < 8$	

The material layout for Reed's problem is given in Table II. We solved this problem by removing the reflecting boundary and doubling the domain so that our region extended from 0 to 16. Using a uniform grid the smallest number of cells that can resolve the material layout is $N_x = 16$ with $\Delta x = 1$. In Figure 1 we display scalar flux solutions to this problem with $N_x = 2^l$ with $l = 4, 6, 8, 10$ (i.e, $16, 64, 256, 4096$) using $K = 2, 3, 4, 6$ to define the number of sub-cells. In this

figure we plot the sub-cell average values. At the lowest resolution there will only be one cell inside the absorber region, where the solution changes most rapidly. The results in Figure 1 demonstrate that at $N_x = 64$ and above for all values of K, the solutions are coincindent on the scale of the graph. Nevertheless, at $N_x = 16$ the solutions differ significantly in the scattering region and absorber. In the scattering region the $K = 2$ solution is too low, the $K = 3$ and 4 solutions appear to be slightly too low at one point, and the $K = 6$ solutions lies on the higher resolution solutions. Similarly, only the $K = 6$ solution is accurate in the absorber. At first blush it may be surprising that one cell can capture the solution in this region. The spectral volume scheme, however, is nearly perfectly designed for this problem. Notice that the only points where the solution is not smooth is at material interfaces. The spectral volume method treats the flow of particles across cell interfaces as not smooth and the interior of the cell as smooth. Therefore, as long as the reconstruction inside the cell can capture the variation in the solution, the spectral volume method will be accurate. In Reed's problem a sixth-order polynomial is sufficient to resolve the solution in the absorber and the scattering region.

Table III: Material Layout for the Diffusive Problem

Isotropic Boundary	Absorbing Region	Strong Scattering Region	Vacuum Boundary
	$\Sigma_a = 2$	$\Sigma_a = 0$	
	$\Sigma_s = 0$	$\Sigma_s = 1000$	
	$0 < x < 1$	$1 < x < 2$	

The next problem we solve has a strongly diffusive region next to an absorber as described in Table III: particles enter the domain with an isotropic distbution, travel two mean-free paths through an absorber and then enter a pure scatterer that is 1000 mean-free paths thick. The solution inside the scattering region will be diffusive, but there is a boundary layer at the material interface. The problem can be described using two spatial cells of constant size. In Figures 2 through 4 we show scalar flux solutions for this problem using $K = 2, 4, 6$ and $N_x = 2, 8, 32, 512$. In each of these figures we use the $K = 6$ and $N_x = 512$ point solution as the comparison solution because this solution resolves a mean-free path in the scatter ($\max \Delta x_{i,k} = .00097656$). This resolved solution demonstrates that the boundary layer at the edge of the scattering region is a sharp, nearly discontinuous, rise from the solution in the absorber. Due to this sharp jump, polynomial approximations of the solution have a difficult time capturing the solution.

The $K = 2$ solution, shown in Figure 2, smooths out the transition from the absorber to the scattering region: the $N_x = 2$ solution is obviously unable to resolve the solution and even the $N_x = 32$ solution under-predicts the maximum value of ϕ in the scattering region. The solution away from the boundary layer is linear with the correct slope for $N_x = 8$ and 32.

In Figure 3, we see that the $K = 4$ solution does a better job of resolving the solution near $x = 1$, including the maximum scalar flux when $N_x = 32$. This better resolution comes at the cost of small oscillations near the boundary layer in all solutions. This is the result of trying to fit the solution using a higher order polynomial: though the solution is smooth, the length scale of the boundary layer is much shorter than the sub-cell widths.

Finally, the $K = 6$ solutions do a better job of capturing the boundary layer, even when there are only two cells in the problem. Nevertheless, as in the $K = 4$ solutions, there are oscillations

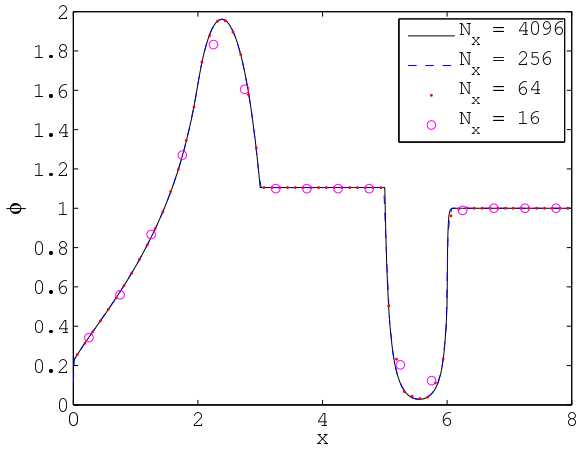

(a) $K = 2$

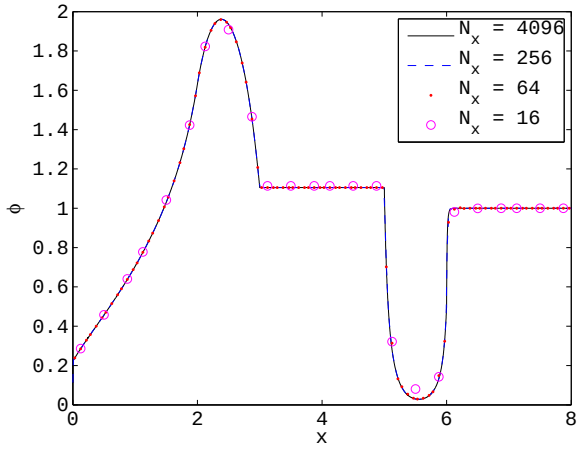

(b) $K = 3$

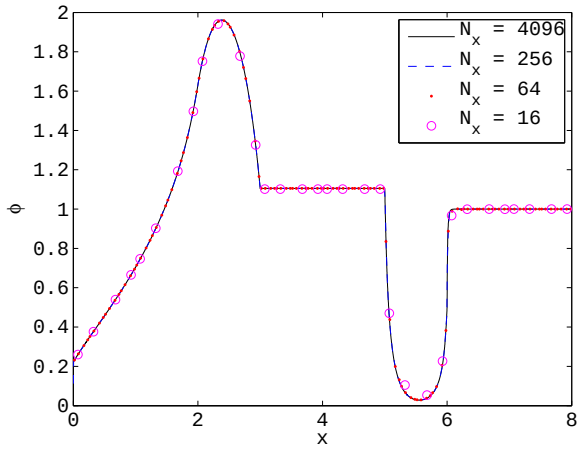

(c) $K = 4$

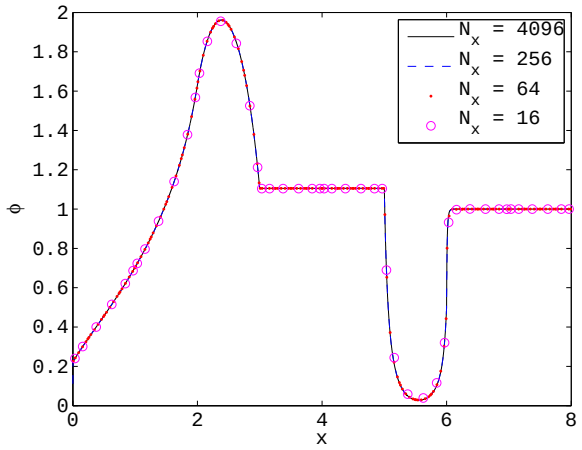

(d) $K = 6$

Figure 1: **Solutions to Reed's problem using various numbers of sub-cells ($K = 2, 3, 4,$ and 6) and several resolutions.**

localized near the boundary layer because a sixth order polynomial is not sufficient to resolve the boundary layer using coarse cells. Despite these oscillations the solution is quite accurate in the boundary layer.

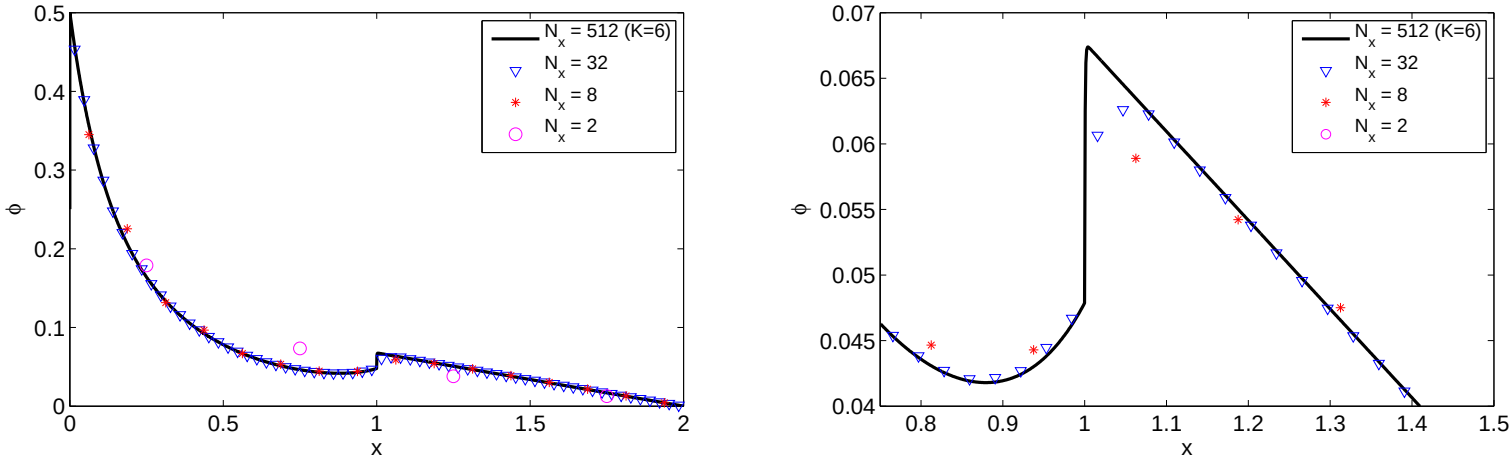

(a) Full domain (b) Detail

Figure 2: Solutions to the diffusive problem with $K = 2$.

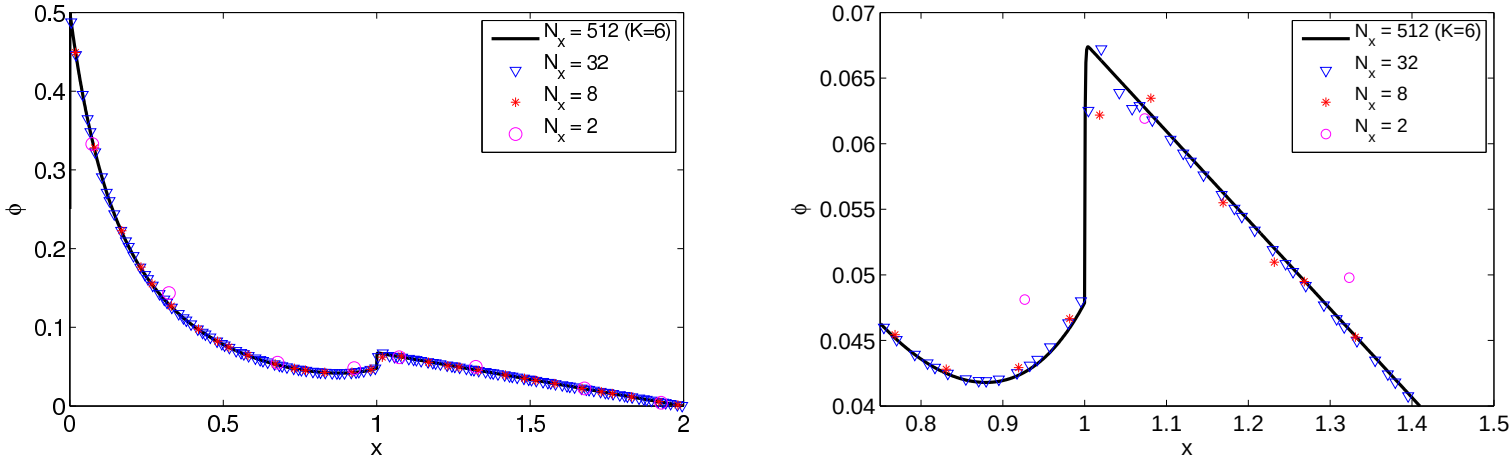

(a) Full domain (b) Detail

Figure 3: Solutions to the diffusive problem with $K = 4$.

5. CONCLUSIONS

We have presented a new discretization for the transport equation that is based on dividing computational cells into sub-cells and using a local polynomial reconstruction. The method can be thought of as a generalization of the simple corner balance method.

Applying the spectral volume method to transport problems demonstrated that the method is robust in the diffusion limit, accurate, and stable. In Reed's problem using the minimum

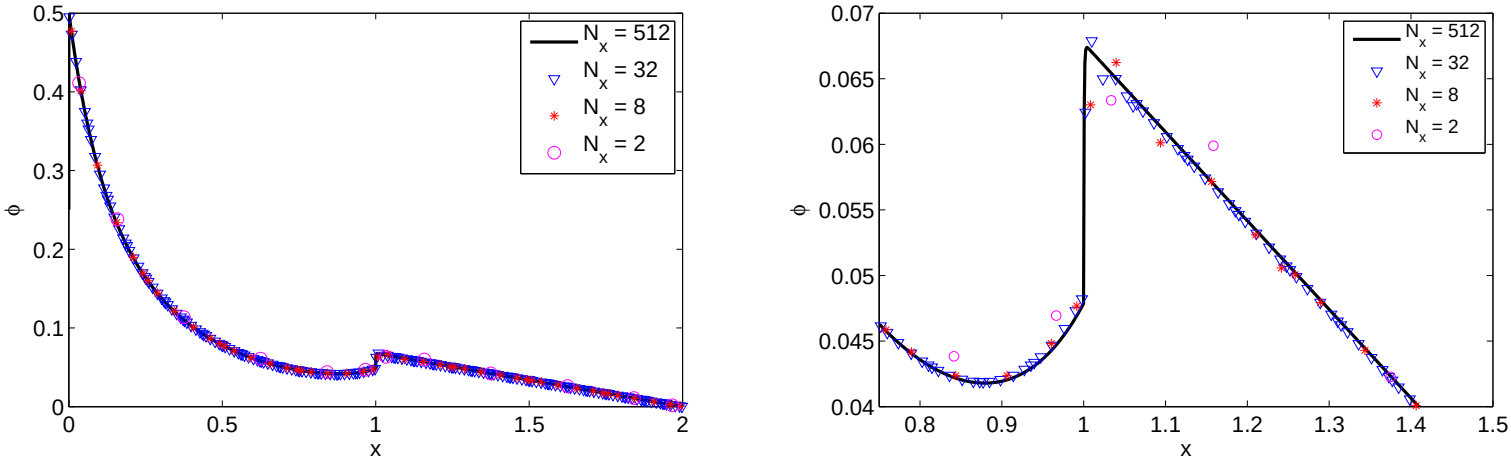

(a) Full domain

(b) Detail

Figure 4: Solutions to the diffusive problem with $K = 6$.

number of uniform cells, the spectral volume method with four and six sub-cells was sufficient to resolve the solution. In a problem with a diffusive boundary layer, the solutions obtained using 4 and 6 sub-cells had small oscillations in the solution, but were able to capture the fine mesh solution behavior in the boundary layer.

Clearly, there are several open questions regarding the spectral volume method. Though we did mention the potential benefits, we did not implement the method on high-performance computing architectures such as multicore or GPU platforms. Indeed, for this method to be viable it must perform well on these platforms. Also, we did not solve multi-dimensional or multigroup problems with the spectral volume method. The method has been successfully applied to multi-dimensional problems in computational fluid dynamics, but there may be unforeseen issues in applying it to transport problems. Finally, applying the method to other angular discretizations than discrete ordinates has yet to be performed. As mentioned above, moment-based methods, such as spherical harmonics, may benefit from eliminating some of the sub-cell unknowns using Schur complements or other techniques.

REFERENCES

1. Marvin L Adams. Discontinuous finite element transport solutions in thick diffusive problems. *Nuclear Science and Engineering*, 137(3):298–333, Jan 2001.

2. Jean Ragusa. Application of h-, p-, and hp-mesh adaptation techniques to the SP_3 equations. *Transp. Th. Stat. Phys.*, 2010. to appear.

3. Z. J. Wang. Spectral (finite) volume method for conservation laws on unstructured grids: Basic formulation. *Journal of Computational Physics*, 178(1):210–251, 2002.

4. Z. J. Wang and Y Liu. Spectral (finite) volume method for conservation laws on unstructured grids II: Extension to two-dimensional scalar equation. *Journal of Computational Physics*, 179(2):665–697, 2002.

5. Z. J. Wang and Y Liu. Spectral (finite) volume method for conservation laws on unstructured grids III: One dimensional systems and partition optimization. *Journal of Scientific Computing*, 20(1):137–157, 2004.

6. Z. J. Wang, L Zhang, and Y Liu. Spectral (finite) volume method for conservation laws on unstructured grids IV: Extension to two-dimensional systems. *Journal of Computational Physics*, 194(2):716–741, 2004.

7. Marvin L Adams. Subcell balance methods for radiative transfer on arbitrary grids. *Transport Theory and Statistical Physics*, 26(4-5):385–431, 1997.

8. E.E. Lewis and W.F. Miller. *Computational Methods of Neutron Transport*. John Wiley and Sons, 1984.

9. Edward W. Larsen, J. E. Morel, and Warren F. Miller. Asymptotic solutions of numerical transport problems in optically thick, diffusive regimes. *Journal of Computational Physics*, 69(2), 1987.

10. T. A. Brunner and Tz. Kolev. Algebraic multigrid for linear systems obtained by explicit element reduction. *SIAM Journal on Scientific Computing*, 2010. in review.

11. G. J. Habetler and B.J. Matkowsky. Uniform asymptotic expansions in transport theory with small mean free paths, and the diffusion approximation. *Journal of Mathematical Physics*, 16(4), April 1975.

12. Edward W. Larsen and Joseph B. Keller. Asymptotic solution of neutron transport problems for small mean free paths. *Journal of Mathematical Physics*, 15(1), January 1974.

13. W. Reed. New difference schemes for the neutron transport equation. *Nucl. Sci. Eng.*, 46:31–39, 1971.

14. J. S. Warsa, T. A. Wareing, and J. E. Morel. Krylov iterative methods and the degraded effectiveness of diffusion synthetic acceleration for multidimensional s-n calculations in problems with material discontinuities. *Nucl. Sci. Eng.*, 147(3):218–248, Jan 2004.